

# The $\pi^0$ mass and the first experimental verification of Coulomb de-excitation in pionic hydrogen

Manfred Daum<sup>\*</sup> and P.-R. Kettle

Paul Scherrer Institut, 5232 Villigen PSI, Switzerland

<sup>\*</sup> [manfred.daum@psi.ch](mailto:manfred.daum@psi.ch)



Review of Particle Physics at PSI  
doi:[10.21468/SciPostPhysProc.5](https://doi.org/10.21468/SciPostPhysProc.5)

## Abstract

The most precise value for the  $\pi^0$  mass was obtained from the measurement of the mass difference  $m_{\pi^-} - m_{\pi^0} = 4.593\,64(48)\text{ MeV}/c^2$  in the charge exchange reaction  $\pi^- p \rightarrow \pi^0 n$  at PSI. With the most precise charged pion mass value,  $m_{\pi^+} = 139.570\,21(14)\text{ MeV}/c^2$  and the validity of the CPT theorem ( $m_{\pi^-} = m_{\pi^+}$ ), a value  $m_{\pi^0} = 134.976\,57(50)\text{ MeV}/c^2$  is obtained. The measurements also revealed, for the first time, evidence of an unexpectedly large contribution from Coulomb de-excitation states during the pionic atom cascade.



Copyright M. Daum and P.-R. Kettle.

This work is licensed under the Creative Commons

[Attribution 4.0 International License](https://creativecommons.org/licenses/by/4.0/).

Published by the SciPost Foundation.

Received 29-05-2021

Accepted 06-07-2021

Published 06-09-2021

doi:[10.21468/SciPostPhysProc.5.012](https://doi.org/10.21468/SciPostPhysProc.5.012)



Check for updates

## 12.1 The mass of the $\pi^0$

One of the main motivations in 1984 for a precision measurement of  $m_{\pi^0}$  was that it allowed for a far more precise comparison between experiment and theory of the rare pion  $\beta$  decay rate  $\Gamma_{\pi\beta}(\pi^+ \rightarrow \pi^0 e^+ \nu)$ , for which the phase space depends on the fifth-power of  $D_\pi = m_{\pi^-} - m_{\pi^0}$ . This required a precision on  $D_\pi$  to better than  $\Delta D_\pi/D_\pi < 0.001$ , a condition that was not met by the world average at the time [1–3].

In this measurement of  $D_\pi$ , negative pions are stopped in a liquid-hydrogen target to form pionic hydrogen atoms. A fraction  $R \approx R_p/(R_p + 1) \approx 0.6$  of these  $\pi^- p$  atoms, where  $R_p$  is the Panofsky ratio [4], undergo the charge-exchange reaction (CEX)

$$\pi^- p \rightarrow \pi^0 n, \quad (12.1)$$

whereas the remaining 40 % of the  $\pi^- p$  atoms undergo radiative capture

$$\pi^- p \rightarrow \gamma n. \quad (12.2)$$

The mass difference  $D_\pi$  is derived from time-of-flight (TOF) distributions of neutrons from reaction (12.1), measured at flight distances of 3.2, 7.9, and 18.1 m. Since the  $\pi^- p$  atoms are

almost at rest, these neutrons generate a TOF peak corresponding to their velocity of about 0.894 cm/ns.

If the  $\pi^-p$  atom is at rest before reaction (12.1), energy and momentum conservation lead to the following equation for the mass difference  $D_\pi$ :

$$D_\pi = m_{\pi^-} - [(m_{\pi^-} - D_N - E_B)^2 - 2(\gamma_{nr} - 1)(m_p + D_N)(m_{\pi^-} + m_p - E_B)]^{1/2}. \quad (12.3)$$

Here,  $D_N \equiv m_n - m_p$  is the nucleon mass difference and  $E_B$  is the binding energy of the  $\pi^-p$  atom just prior to reaction (12.1). The rest mass of the  $\pi^-p$  atom is  $m_{\pi p} = m_{\pi^-} + m_p - E_B$ ;  $\gamma_{nr} \equiv (1 + \beta_{nr}^2)^{-1/2}$  is the usual function of the neutron velocity  $v_{nr} = c\beta_{nr}$  for  $\pi^-p$  atoms at rest; we set  $c = 1$ , except where the units are given explicitly.

From (12.3) it follows that the experimental uncertainty of  $D_\pi$  contains five contributions,  $\beta_{nr}$ ,  $m_{\pi^-}$ ,  $m_p$ ,  $D_N$ , and  $E_B$ , see [5–7], resulting in a relative uncertainty of  $D_\pi$  of the same order as that of  $\beta_{nr}$ :

$$(\Delta D_\pi)_{\beta_{nr}} / D_\pi = 1.46 \Delta \beta_{nr} / \beta_{nr}. \quad (12.4)$$

The remaining four contributions can be neglected, see [7]. Thus, the experiment consists of determining the velocity of the neutron from the charge-exchange reaction (12.1).

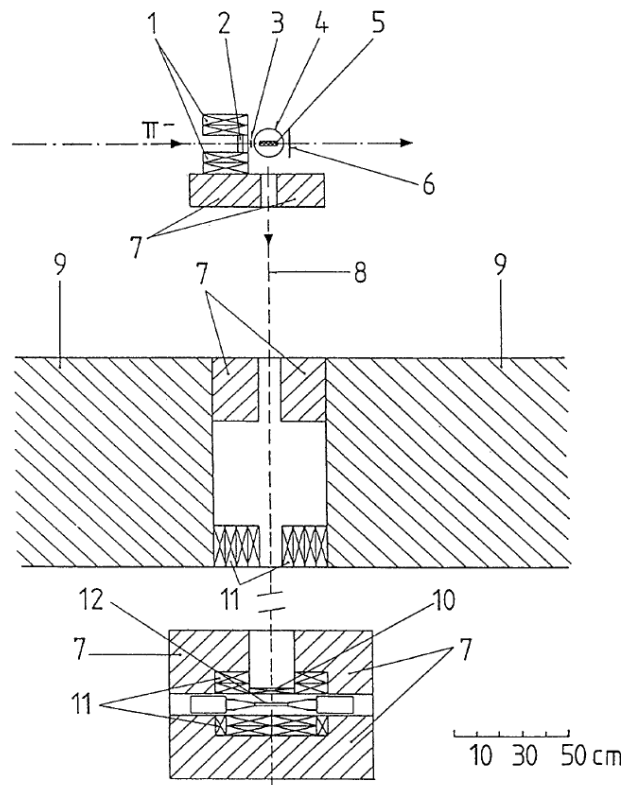


Figure 12.1: Experimental setup: (1) lead collimator; (2) CH<sub>2</sub> degrader; (3) Scintillator S<sub>1</sub>; (4) vacuum chamber of the liquid hydrogen target; (5) liquid hydrogen target; (6) scintillator S<sub>2</sub>; (7) CH<sub>2</sub> shielding; (8) central neutron trajectory; (9) concrete shielding; (10) lead converter; (11) lead collimator; (12) Scintillator S<sub>3</sub>.

The measurements were made at the 590 MeV proton accelerator at PSI. The experimental layout is shown in Figure 12.1. Negative pions with a momentum of 120 MeV/c were transported by the secondary beam line  $\pi E1$  to a liquid hydrogen target assembly. At that

momentum, the substantial electron contamination in the beam was suppressed using time-of-flight (TOF), by requiring a coincidence between the scintillator  $S_1$  and the radio frequency signal of the accelerator.

The pions passed through a  $\text{CH}_2$  degrader, optimized to maximize the pion stopping rate in the liquid hydrogen. The hydrogen was contained in a cylindrical stainless steel cell with a length of 1.6 cm and a radius of 4.5 cm, oriented so that the cylinder axis coincided with the neutron flight direction, see Figure 12.1.

The incoming pions were detected by a plastic scintillator  $S_1$  in anti-coincidence with the scintillator  $S_2$ . The coincidence  $(S_1 \cdot \text{rf}) \cdot (S_2 \cdot \text{rf})$  indicated a stopping pion. Neutrons and photons from the liquid hydrogen target were observed after a flight path of variable length (3-18 m) defined by a series of  $\text{CH}_2$  and Pb collimators.

The neutrons and photons from reactions (12.1) and (12.2) were detected by a NE102A organic scintillator  $S_3$  of thickness 1.6 cm viewed from opposite sides through lucite light guides by two photomultipliers. The neutron detector was shielded by  $\text{CH}_2$  and lead as shown in Figure 12.1. The neutron detector assembly was mounted on a steel cart equipped with optical targets for surveying.

Data were taken with the neutron detector at three distances from the nominal hydrogen target location: (i) 3.1966 m, (ii) 7.9283 m, and (iii) 18.1005 m. The distance between positions (i) and (ii) was determined to  $\pm 0.1$  mm and that between positions (i) and (iii) to  $\pm 0.4$  mm. For more information see [7].

The method of determining the neutron velocity is similar to that of [1]. However, the older method depended on the measurement of signal velocities in the coaxial delay cables, whereas in our case this time standard is replaced by the precisely known radio frequency structure of the pion beam. The neutron velocity  $v_{nr}$  from the charge exchange reaction (12.1) is derived from the position of the neutron peak in the TOF spectra (Figure 12.2) relative to the pattern of the accidental photon peaks. These peaks appear at regular intervals of  $\tau_{rf} = (19.750\,034 \pm 0.000\,002)$  ns.

The raw time distribution of the events, as recorded by a time-to-digital converter (TDC) at a flight path of 7.9 m, is shown in Figure 12.2. The data are shown in Figure 12.3 after background subtraction, for all three distances.

Neglecting the fact that the  $\pi^-p$  atoms have a finite kinetic energy  $T_{\pi p}$  and are in different atomic states at the time of reaction (12.1), all neutrons from that reaction would have the same velocity,  $v_{nr}$ , which is related to the particle masses by energy and momentum conservation ( $c = 1$ )

$$m_{\pi p} = E_n + E_{\pi^0} = \sqrt{m_n^2 + p_n^2} + \sqrt{m_{\pi^0}^2 + p_{\pi^0}^2}. \quad (12.5)$$

Here,  $E_n$  and  $E_{\pi^0}$  are the total neutron and  $\pi^0$  energies, respectively, and  $p_n = m_n \beta_{nr} \gamma_{nr}$  is the neutron momentum.

Without the assumption of the initial  $\pi^-p$  atoms being at rest, the predicted neutron TOF distribution  $F(\tau)$  for a given neutron flight path  $l_n$  has a finite width. It can be shown [7] that, for an isotropic distribution of the  $\pi^-p$  atom velocities, the mean of the neutron TOF distribution is equal to the TOF for  $\pi^-p$  atoms at rest. The standard deviation of the function  $F(\tau)$  is [7]

$$\sigma_\tau = (2\overline{T_{\pi p}}/3m_{\pi p})^{1/2} l_n / v_{nr}^2, \quad (12.6)$$

where  $\overline{T_{\pi p}}$  is the mean kinetic energy of the  $\pi^-p$  atom. It is seen from (12.6) that the standard deviation of the TOF distribution function  $F(\tau)$  increases linearly with the neutron flight path  $l_n$ .

The broadening of the TOF peaks with increasing flight path is indeed observed in the spectra of Figure 12.3. The tails to the right of the neutron peaks, i.e., to longer times-of-flight, are due not only to the finite kinetic energy of the  $\pi^-p$  atoms but also to neutrons which have

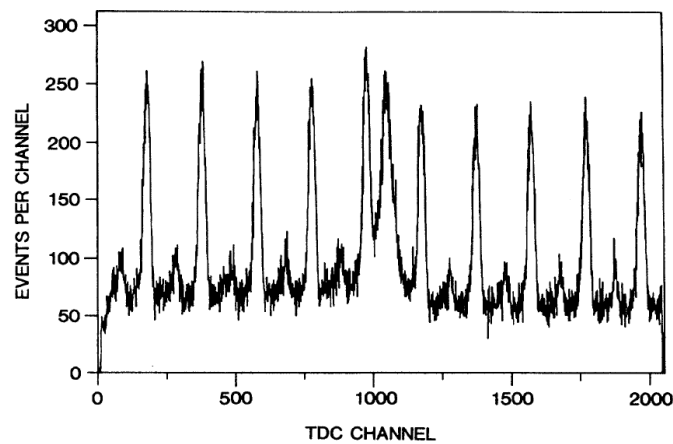


Figure 12.2: Uncorrected time spectrum recorded at a flight path of  $l = 7.9$  m. Abscissa: TDC channel number for  $S_3$ ; channel  $\approx 0.1$  ns. Ordinate: number of events per channel. This distribution contains three classes of events: (a) The peak at channel 1040 of Figure 12.2 is due to neutrons from the charge exchange reaction (12.1). (b) The narrow peaks at channels 180, 380, 580, ..., are due to photons from the  $\pi^0$  decay following reaction (12.1) and photons from reaction (12.2). (c) The small peaks about halfway between the photon peaks, i.e., at channels 80, 280, 480, ..., originate from accidental events in which the TDC was started by a neutron detector signal due to beam electrons scattered in the liquid hydrogen target assembly.

reached the detector after scattering in the materials in and around the flight channel. In contrast, the tails to the left are not contaminated by neutron scattering. The tail visible at 3.2 m, extends to about 10 ns (20 ns) before the peak at 7.9 m (18.1 m), corresponding to an energy distribution  $f(T_{\pi p})$  extending to about 70 eV.

The curves in Figure 12.3 were obtained by fitting nine free parameters simultaneously to all three experimental spectra, for details see [7]. An energy distribution found to fit the data is shown in Figure 12.4 together with the corresponding neutron TOF distribution  $F(\tau)$  for a fixed flight path of 18.1 m. The  $\chi^2$  of the fit shown in Figure 12.3 is 1265 for 1191 degrees of freedom.

The resulting neutron velocity from the charge exchange reaction (12.1) and for the  $\pi^- p$  atom at rest is

$$v_{nr} = (0.894\,266 \pm 0.000\,063) \text{ cm/ns.} \quad (12.7)$$

The corresponding mass difference is

$$D_\pi = m_{\pi^-} - m_{\pi^0} = (4.593\,64 \pm 0.000\,48) \text{ MeV}/c^2. \quad (12.8)$$

This result agrees with our previous measurement [5]. The deviation from the former world average [3], ( $D_\pi = 4.604\,3 \pm 0.003\,7$ ) MeV/ $c^2$ , which was dominated by the values of [1,2] is thus confirmed at a level of  $2.9\sigma$ . Assuming the validity of the CPT theorem ( $m_{\pi^+} = m_{\pi^-}$ ), subtracting the mass difference (12.8) from the charged pion mass [8],  $m_{\pi^+} = 139.570\,21(14)$  MeV/ $c^2$  gives the new  $\pi^0$  mass value,

$$m_{\pi^0} = (134.976\,57 \pm 0.000\,50) \text{ MeV}/c^2. \quad (12.9)$$

A similar analysis based on the fast neutron TOF spectra from the simultaneously measured radiative capture reaction (12.2) results in a value for the negative pion mass, consistent with

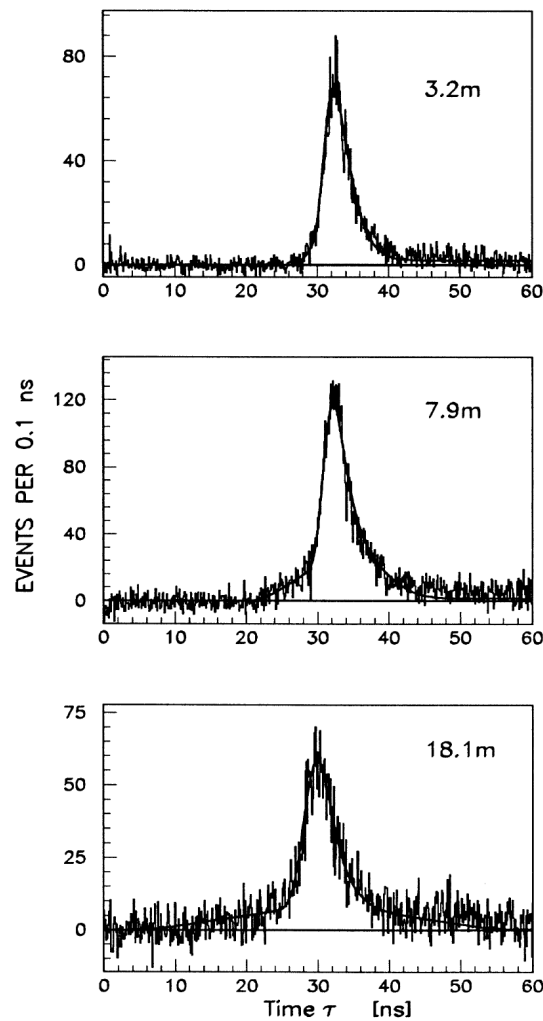


Figure 12.3: Experimental TOF spectra of neutrons from the charge exchange reaction  $\pi^- p \rightarrow \pi^0 n$ , after background subtraction, for flight paths of 3.2 m, 7.9 m, and 18.1 m. The time shown is from an accidental photon peak about 30 ns before the neutron peak. Curves: theoretical distributions fitted to the data, c.f. [7].

the world average value, albeit with reduced precision. As the dominant uncertainty is from the neutron velocity, this provides evidence of the validity of the velocity analysis method used.

The fit also allows the extraction of the corresponding mean kinetic energy of the  $\pi^- p$  atom

$$\overline{T_{\pi p}} = (16.2 \pm 1.3) \text{ eV} \quad (12.10)$$

confirming the strong deviation from the velocity spread quoted in [1] which corresponded to  $\overline{T_{\pi p}} = (115 \pm 43) \text{ eV}$ .

## 12.2 First experimental verification of Coulomb de-excitation in pionic hydrogen

The TOF-data for the  $D_\pi$  measurement show a Doppler broadening of the neutron peaks with increasing flight distance, attributed to 'high-energy' pionic atoms at the time of the CEX-reaction. Further evidence for this was reported later by an experiment in gaseous hydrogen [9].

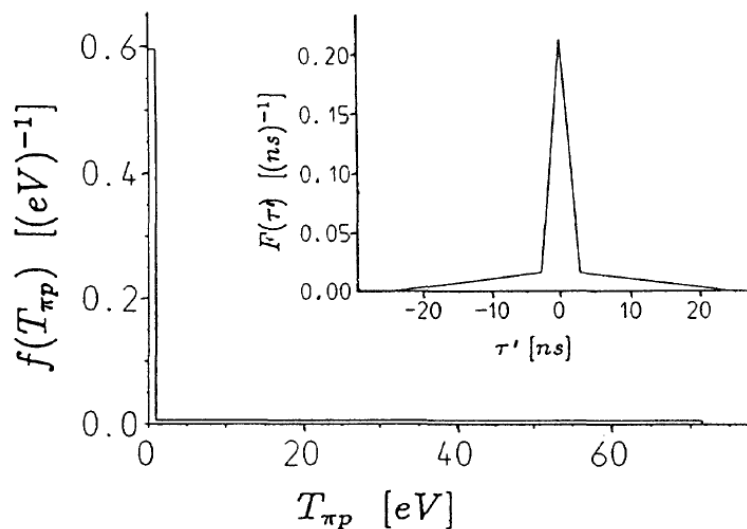


Figure 12.4: Model distribution function  $f(T_{\pi p})$  found to fit the neutron TOF spectra of Figure 12.3;  $T_{\pi p}$  is the kinetic energy of the  $\pi^-p$  atom just prior to the charge exchange reaction (12.1);  $F(\tau')$  is the corresponding neutron TOF distribution for a flight path of 18.1 m.

The kinetic energy distribution  $f(T_{\pi p})$  and the corresponding TOF-distribution  $F(\tau)$  for this simple model for the  $D_\pi$ -data was further refined in a new experiment, undertaken to prove the existence of the Coulomb de-excitation process [10, 11] in liquid and gaseous hydrogen, and to determine if it is responsible for the broadening. A further aim was to verify that the multi-component structure of the kinetic energy distribution is associated with this process.

The motivation for this experiment was to test the cross-section predictions for various cascade processes for exotic hydrogen atoms, which are important for experiments such as pionic X-ray transition measurements to determine the ground state strong interaction width [12–14] and the effect of the Doppler broadening of pionic X-ray lines in the determination of the pion-nucleon scattering lengths. The most likely process capable of producing such a broadening effect is Coulomb de-excitation [10, 11]. Here,  $(\pi^-p)_n + p \rightarrow (\pi^-p)_{n'} + p$  where the smaller neutral pionic atom collides with a proton of a hydrogen atom causing a transition of the pionic atom, whereby the de-excitation energy is shared between the collision partners. Other possible processes either reduce  $T_{\pi p}$  or leave it almost unchanged. Coulomb de-excitation predictions calculated by several authors [11, 15–17] vary by more than an order-of-magnitude so that precise data are necessary to test the predictions.

Here we outline the new experiment, concentrating on the liquid hydrogen results [18]. Several experimental improvements [5–7] were implemented:

1. Background reduction and increased statistics by use of (i) an extra neutron collimator system close to the target, (ii) an array of neutron counters with specially selected low-noise photomultipliers, and (iii) a 64-counter array of NaI photon counters for tagging the neutrons from reactions (12.1) and (12.2).
2. Improved time-resolution, by reducing both the thickness of the neutron detectors and the liquid hydrogen cell [18, 19].

In this experiment, negative pions of 117 MeV/c were slowed down in a carbon degrader and stopped in a liquid hydrogen target. Neutrons from reaction (12.1) were detected for

various flight-path lengths between 3 and 11 m. Time-of-flight and pulse-height data were recorded by time-to-digital (TDC) and analogue-to-digital (ADC) convertors.

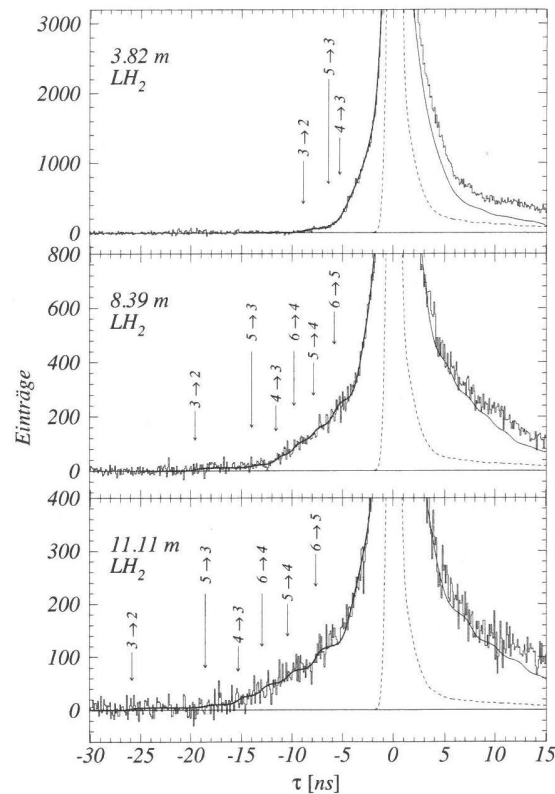


Figure 12.5: Neutron time-of-flight spectra from the charge exchange reaction  $\pi^-p \rightarrow \pi^0n$  in a liquid hydrogen target ( $LH_2$ ). The time is measured from the centre of the neutron peak corresponding to the reaction at rest. Solid curves: fit to the data including Coulomb de-excitation processes. The numbers  $n \rightarrow n'$  indicate the expected positions of the steps in the TOF distribution of neutrons emitted after the corresponding Coulomb de-excitation. Dashed line: unbroadened neutron TOF distribution from Monte Carlo program.

Figure 12.5 shows the neutron TOF-spectra taken at 3.82 m, 8.39 m and 11.11 m, after background subtraction and pulse-height cuts to remove noise and accidental photon events from  $\pi^0$ -decay and radiative capture, as well as bremsstrahlung events from beam electrons. Further energy cuts (between 60 and 110 MeV) on the photon detected in the NaI array eliminated both bremsstrahlung and radiative capture events. Figure 12.5 shows a clear distance-dependent broadening of the neutron line shape, when compared to the Monte Carlo generated intrinsic line shape.

The data of Figure 12.5 were analyzed by applying three fitting procedures; two based on the full model of Coulomb de-excitation shown in Figure 12.6 - one including both  $\Delta n = 1$  and  $\Delta n = 2$  pionic atom transitions in the fitted  $F(\tau)$  distributions and one including only the  $\Delta n = 1$  transitions. The third procedure used the simplified model of Figure 12.4 for comparison.

Clear step-like structures in the data at 3.8 m and 8.4 m can be seen reaching to  $-9$  ns and  $-20$  ns, respectively, corresponding to the  $\Delta n = 1$  transition  $3 \rightarrow 2$  having a kinetic energy of 209 eV. A second component visible at all three distances corresponding to  $-6$  ns,  $-12$  ns and  $-15$  ns, signals the  $\Delta n = 1$  transition  $4 \rightarrow 3$  in the pionic atom with a kinetic energy of about

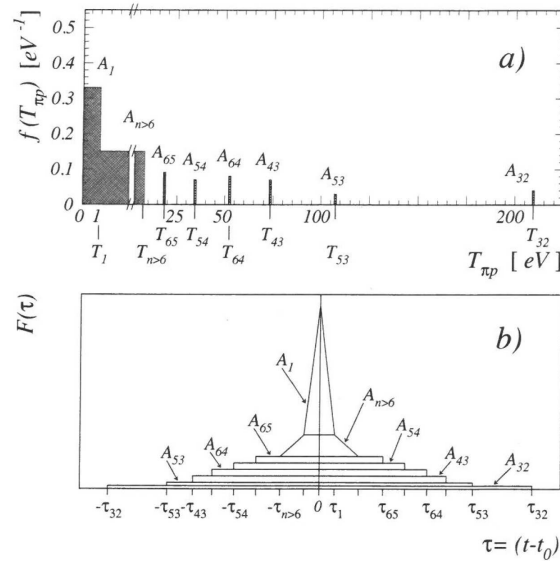


Figure 12.6: (a) Idealized distribution function  $f(T_{\pi p})$  of the kinetic energy  $T_{\pi p}$  of pionic hydrogen atoms at the instant of nuclear capture. For clarity,  $T_1$  and the widths of the four  $\delta$ -like peaks at  $T_{nn'}$  are drawn to be 1 eV. The energy distribution  $f(T_{n>6})$  is about 7 eV wide and describes all transitions  $n \rightarrow n'$  with  $n > 6$ . The integrals of these distributions and peaks correspond to the relative yields  $A_1$ ,  $A_{nn'}$  and  $A_{n>6}$ , respectively. (b) Neutron TOF-distribution  $F(\tau)$  corresponding to the kinetic energy distribution of Fig. 1(a).

70 eV.

The final results from the experiment for the kinetic energy distribution for pionic hydrogen, based on Coulomb de-excitation transitions, are shown in Table 12.1, for both liquid and gaseous hydrogen and are based on the three independent fits [18]. Although visually, the significance of the steps in the TOF-spectra is only fair, their true significance can be seen from the fit results in the table, when the theoretical model of Figure 12.6 is fitted simultaneously to all three TOF spectra. Here, a 16-parameter fit of the model-based TOF spectra are fitted to the measured distributions and involve: (i) four yields from  $\Delta n = 1$  transition  $6 \rightarrow 5$ ,  $5 \rightarrow 4$ ,  $4 \rightarrow 3$  and  $3 \rightarrow 2$ ; (ii) two yields for  $\Delta n = 2$  transitions  $6 \rightarrow 4$  and  $5 \rightarrow 3$ ; (iii) one yield and one upper energy bound for  $n > 6$  transitions; (iv) the energy parameter  $T_1$  for the low-energy component; (v) a distance independent Gaussian electronic time-jitter [7]; (vi) three normalization factors for the ordinates; (vii) three time shifts ( $0.3 \pm 0.1$ ) channels, as free parameters.

The fits incorporating the  $\Delta n = 1$  and  $\Delta n = 2$  transitions gave a  $\chi^2/\text{DOF}$  of 0.96 with 740 degrees of freedom (DOF); this corresponds to a confidence level of 77.7%. The data were also fitted with the parameterization of [7] (two uniform kinetic-energy distributions of the  $\pi^-p$ -atom, cf. Figure 12.4). In this case, the resulting  $\chi^2$  was 2.43/DOF (cf. also [19]). The poor fit due to this parameterization originates from the lack of discrete components, e.g. the  $3 \rightarrow 2$  transition.

For comparison, fits were also made excluding the Coulomb de-excitation components with  $\Delta n = 2$ . These fits gave a  $\chi^2/\text{DOF}$  of 1.06 with 742 DOF which corresponds to a confidence level of 13.1%. The differences in the  $\chi^2/\text{DOF}$  between the fits with and without  $\Delta n = 2$  transitions are not very significant; however, there is strong evidence for components with  $\Delta n = 2$  from the two other model-independent methods used in the analysis to extract the



Table 12.1: Fitted yields  $A_{nn'}$  of Coulomb de-excitation peaks in the kinetic energy distribution  $f(T_{\pi p})$  for the transitions  $n \rightarrow n'$  in liquid and gaseous hydrogen. Fit results including  $\Delta n = 2$  (left) and  $\Delta n = 1$  only (right).

transition	energy $T_{nn'}$ [eV]	$A_{nn'}$ [%]			
		LH <sub>2</sub>	H <sub>2</sub> gas	LH <sub>2</sub>	H <sub>2</sub> gas
$n > 6$	< 18.4	$27 \pm 2$	$19 \pm 5$	$26 \pm 2$	$21 \pm 5$
$6 \rightarrow 5$	18.4	$9 \pm 1$	$9 \pm 3$	$7 \pm 1$	$6 \pm 3$
$5 \rightarrow 4$	33.9	$7 \pm 1$	$7 \pm 4$	$12 \pm 1$	$14 \pm 3$
$4 \rightarrow 3$	73.2	$7 \pm 1$	$5 \pm 3$	$14 \pm 1$	$10 \pm 2$
$3 \rightarrow 2$	209.1	$3 \pm 1$	$5 \pm 1$	$4 \pm 1$	$4 \pm 1$
$6 \rightarrow 4$	52.3	$8 \pm 1$	$9 \pm 4$	/	/
$5 \rightarrow 3$	107.1	$3 \pm 1$	$0_{-0}^{+2}$	/	/
$\chi^2/\text{DOF}$		0.96	0.96	1.06	0.96
$T_1$ [eV]		$1.0 \pm 0.1$	$1.6 \pm 0.2$	$1.0 \pm 0.1$	$1.5 \pm 0.3$
$A_1$ [%]		$36 \pm 2$	$46 \pm 6$	$36 \pm 2$	$45 \pm 6$
$T_{n>6}$ [eV]		$7.6 \pm 0.3$	$6.7 \pm 2.2$	$7.9 \pm 0.4$	$6.8 \pm 2.3$

kinetic energy distribution  $f(T_{\pi p})$  from the data, see [18]. In addition, the difference between the predicted and the observed transition energies  $T_{nn'}$  reported in [19] can be accounted for and made to vanish in our present analysis if we include the  $\Delta n = 2$  Coulomb de-excitation transitions. Then, the resultant energies  $T_{nn'}$  for  $n \leq 6$  perfectly match the theoretical values derived from the Coulomb de-excitation model and do not have to be taken as free parameters. This is considered as a strong indication of the existence of the  $\Delta n = 2$  Coulomb de-excitation transitions.

In conclusion, the first estimates of the Coulomb de-excitation were made by Bracci and Fiorentini [11]. They were criticized by Ponomarev and Solov'ev [17] who obtained significantly smaller Coulomb de-excitation rates which, however, disagreed with the experimental results [18, 19] and this paper. Significant progress came with the more advanced theoretical calculations by Popov and Pomerantsev [20]. The cascade calculations using these cross sections predict a substantial high-energy component. Finally, Hirtl et al. [21] state that the theoretical prediction for the kinetic energy distributions and the experimental results do not show any drastic inconsistencies.

## References

- [1] J. B. Czirr, *Determination of  $\pi$ -meson masses by neutron time of flight*, Phys. Rev. **130**, 341 (1963), doi:[10.1103/PhysRev.130.341](https://doi.org/10.1103/PhysRev.130.341).
- [2] I. M. Vasilevsky, V. V. Vishnyakov and A. F. Dunaitsev, *Mass difference of the negative and neutral pions*, Phys. Lett. **23**, 281 (1966), doi:[10.1016/0031-9163\(66\)90184-3](https://doi.org/10.1016/0031-9163(66)90184-3).
- [3] M. Aguilar-Benitez et al., *Review of particle properties. Particle Data Group*, Phys. Lett. B **170**, 1 (1986).
- [4] W. K. H. Panofsky, R. L. Aamodt and J. Hadley, *The gamma-ray spectrum resulting from capture of negative  $\pi$ -mesons in hydrogen and deuterium*, Phys. Rev. **81**, 565 (1951), doi:[10.1103/PhysRev.81.565](https://doi.org/10.1103/PhysRev.81.565).

- [5] J. F. Crawford, M. Daum, R. Frosch, B. Jost, P. R. Kettle, R. M. Marshall and K. O. H. Ziock, *Precision measurement of the mass difference  $m_{\pi^-} - m_{\pi^0}$* , Phys. Rev. Lett. **56**, 1043 (1986), doi:[10.1103/PhysRevLett.56.1043](https://doi.org/10.1103/PhysRevLett.56.1043).
- [6] J. F. Crawford, M. Daum, R. Frosch, B. Jost, P. R. Kettle, R. M. Marshall, B. K. Wright and K. O. H. Ziock, *Precision measurement of the mass difference  $m_{\pi^-} - m_{\pi^0}$* , Phys. Lett. B **213**, 391 (1988), doi:[10.1016/0370-2693\(88\)91782-0](https://doi.org/10.1016/0370-2693(88)91782-0).
- [7] J. F. Crawford, M. Daum, R. Frosch, B. Jost, P. R. Kettle, R. M. Marshall, B. K. Wright and K. O. H. Ziock, *Precision measurement of the pion mass difference  $m_{\pi^-} - m_{\pi^0}$* , Phys. Rev. D **43**, 46 (1991), doi:[10.1103/PhysRevD.43.46](https://doi.org/10.1103/PhysRevD.43.46).
- [8] M. Daum, R. Frosch and P. R. Kettle, *The charged and neutral pion masses revisited*, Phys. Lett. B **796**, 11 (2019), doi:[10.1016/j.physletb.2019.07.027](https://doi.org/10.1016/j.physletb.2019.07.027).
- [9] E. C. Aschenauer *et al.*, *Cascade processes and the kinetic-energy distribution of pionic hydrogen atoms*, Phys. Rev. A **51**, 1965 (1995), doi:[10.1103/PhysRevA.51.1965](https://doi.org/10.1103/PhysRevA.51.1965).
- [10] M. Leon and H. A. Bethe, *Negative meson absorption in liquid hydrogen*, Phys. Rev. **127**, 636 (1962), doi:[10.1103/PhysRev.127.636](https://doi.org/10.1103/PhysRev.127.636).
- [11] L. Bracci and G. Fiorentini, *Coulomb deexcitation of mesic hydrogen*, Nuovo Cim. A **43**, 9 (1978), doi:[10.1007/BF02729003](https://doi.org/10.1007/BF02729003).
- [12] W. Beer *et al.*, *Determination of the strong interaction shift in pionic hydrogen with a high resolution crystal spectrometer system*, Phys. Lett. B **261**, 16 (1991), doi:[10.1016/0370-2693\(91\)91317-0](https://doi.org/10.1016/0370-2693(91)91317-0).
- [13] D. Sigg *et al.*, *The Strong interaction shift and width of the 1S level in pionic hydrogen*, Phys. Rev. Lett. **75**, 3245 (1995), doi:[10.1103/PhysRevLett.75.3245](https://doi.org/10.1103/PhysRevLett.75.3245).
- [14] D. Sigg *et al.*, *The strong interaction shift and width of the ground state of pionic hydrogen*, Nucl. Phys. A **609**, 269 (1996), doi:[10.1016/S0375-9474\(96\)00280-1](https://doi.org/10.1016/S0375-9474(96)00280-1), [Erratum: Nucl. Phys. A **617**, 526 (1997)].
- [15] L. Men'shikov, *Mesic atom acceleration mechanisms in cascade transitions*, Muon Catalyzed Fusion **2**, 173 (1988).
- [16] W. Czaplinski, A. Gula, A. Kravtsov, A. Mikhailov and N. Popov, *Kinetics of excited muonic hydrogen*, Phys. Rev. A **50**, 525 (1994), doi:[10.1103/PhysRevA.50.525](https://doi.org/10.1103/PhysRevA.50.525).
- [17] L. I. Ponomarev and E. A. Solov'ev, *Cascade acceleration of  $p\pi$  atoms in the Coulomb deexcitation process*, J. Exp. Theor. Phys. Lett. **64**, 135 (1996), doi:[10.1134/1.567164](https://doi.org/10.1134/1.567164).
- [18] A. Badertscher, P. F. A. Goudsmit, M. Janousch, Z. G. Zhao, M. Daum, P. R. Kettle, V. E. Markushin, J. Schottmueller and J. Koglin, *Experimental verification of Coulomb deexcitation in pionic hydrogen*, Europhys. Lett. **54**, 313 (2001), doi:[10.1209/epl/i2001-00243-1](https://doi.org/10.1209/epl/i2001-00243-1).
- [19] A. Badertscher, M. Daum, R. Frosch, P. F. A. Goudsmit, W. Hajdas, M. Janousch, P. R. Kettle, V. Markushin, J. Schottmuller and Z. G. Zhao, *Experimental determination of the kinetic energy distribution of  $\pi^- p$  atoms in liquid hydrogen*, Phys. Lett. B **392**, 278 (1997), doi:[10.1016/S0370-2693\(96\)01545-6](https://doi.org/10.1016/S0370-2693(96)01545-6).
- [20] V. P. Popov and V. N. Pomerantsev, *Kinetic energy distributions of muonic and pionic hydrogen atoms*, Hyperfine Interact. **209**, 75 (2012), doi:[10.1007/s10751-011-0514-2](https://doi.org/10.1007/s10751-011-0514-2).
- [21] A. Hirtl *et al.*, *Redetermination of the strong-interaction width in pionic hydrogen*, Eur. Phys. J. A **57**, 70 (2021), doi:[10.1140/epja/s10050-021-00387-x](https://doi.org/10.1140/epja/s10050-021-00387-x).